Extrapolation of Missing Craniofacial Skeletal Structure via Statistical Shape Models

Project #1 Seminar Presentation

EN.600.646 Spring 2014

Robert Grupp

Hsin-Hong Chiang

Dr. Yoshito Otake (Mentor)

Dr. Russell Taylor (Mentor)

Dr. Mehran Armand (Mentor)

Ryan Murphy (Mentor)

Johns Hopkins Whiting School of Engineering

cisst

ERC | CISST

Collaborative Laboratory for BIGSS Biomechanical- and Image-guided Surgical Systems

Laboratory for Computational Sensing + Robotics, The Johns Hopkins University

Project Overview

- *Project Goal:* Design and implement a method for extrapolating missing anatomical craniofacial skeletal structure with the use of a statistical shape model of the human cranium.

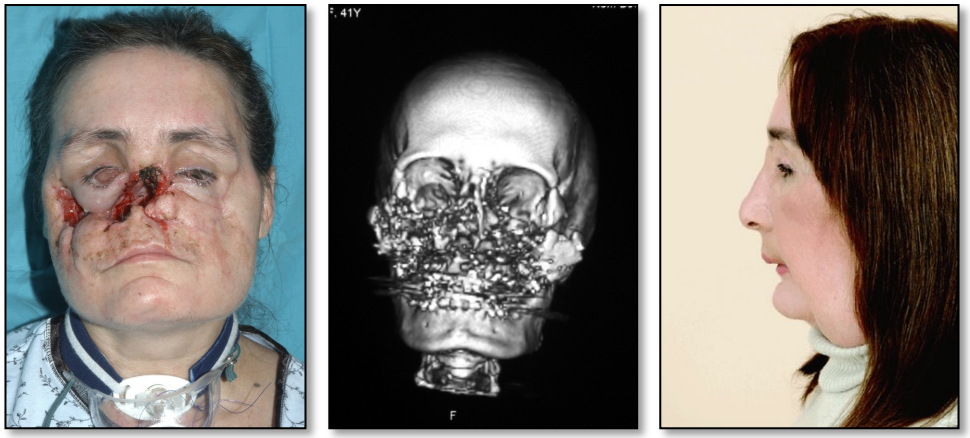

Courtesy of Dr. Chad Gordon

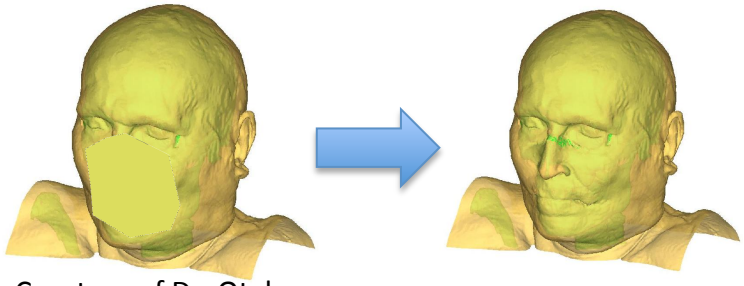

Courtesy of Dr. Otake

Today's Papers

- S. Benazzi and S. Senck. **Comparing 3-Dimensional Virtual Methods for Reconstruction in Craniomaxillofacial Surgery**. *Journal of Oral and Maxillofacial Surgery*, 69(4):1184 – 1194, 2011.
- M. Kazhdan, M. Bolitho, and H. Hoppe. **Poisson Surface Reconstruction**. In *Proceedings of the fourth Eurographics symposium on Geometry processing*, 2006.

Motivation

- We expect that the atlas based extrapolation proposed by Chintalapani, will have some discontinuities

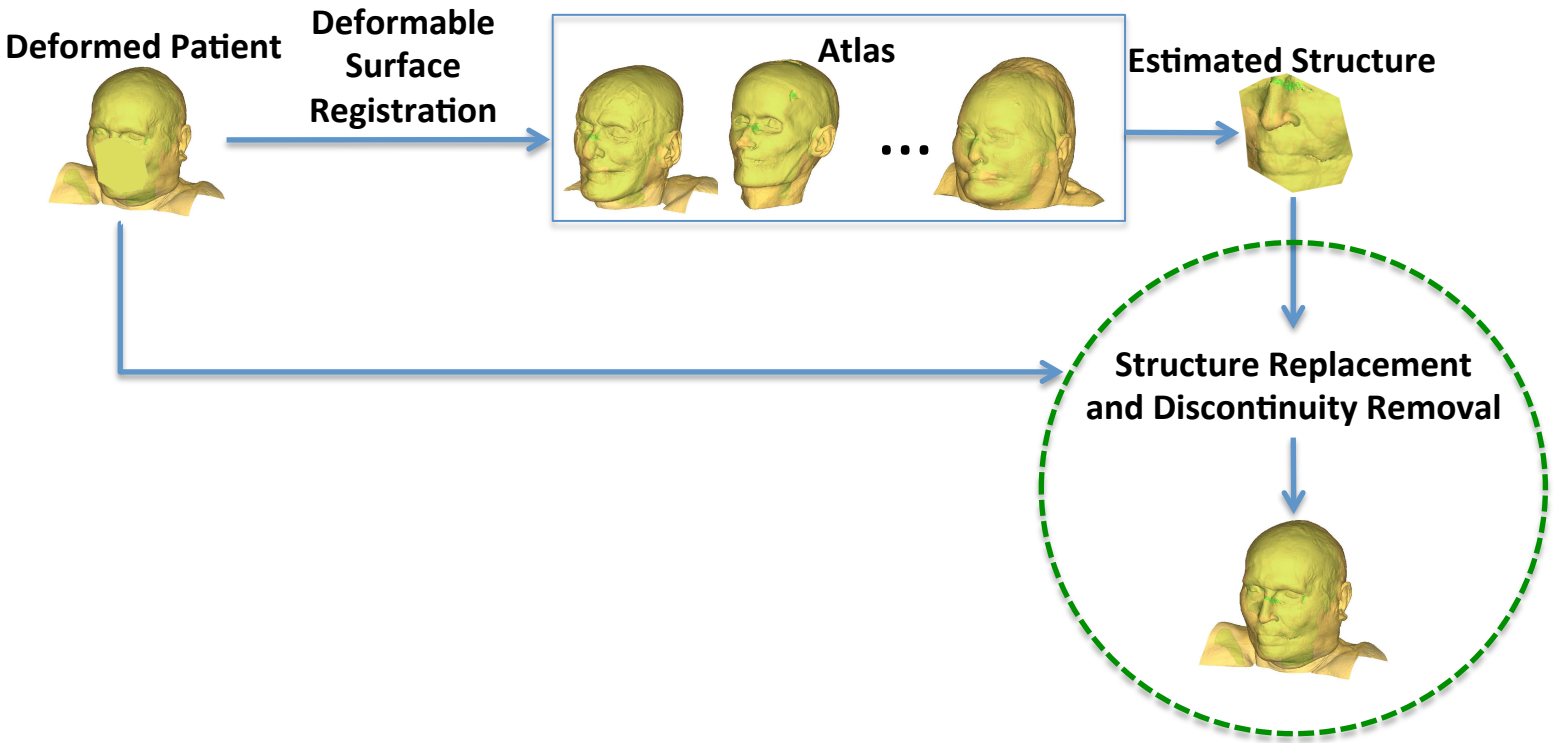

Cadaver CT Courtesy of Dr. Otake

Benazzi, et al. Introduction

- Comparing 3-Dimensional Virtual Methods for Reconstruction in Craniomaxillofacial Surgery
  - Describes 3 methods for reconstructing missing anatomy as a result of a virtual osteotomy for 15 different virtual patients

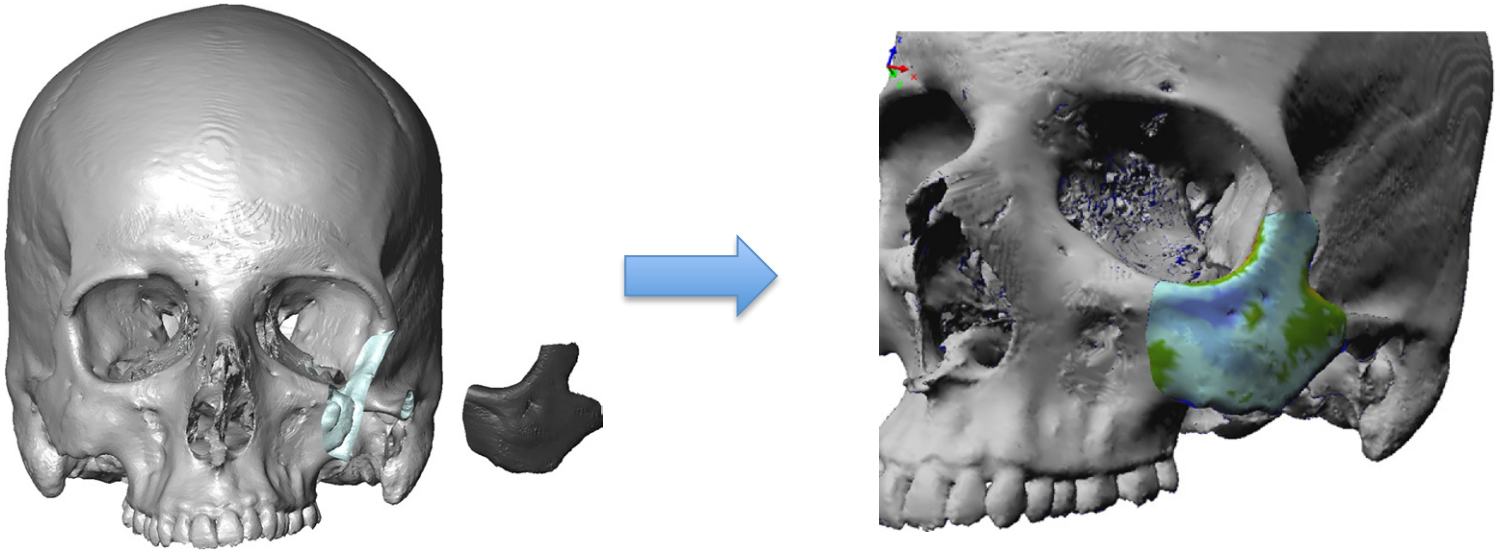

Benazzi and Senck. 3D Virtual Methods for Craniomaxillofacial Reconstruction. J Oral Maxillofac Surg 2011.

Benazzi, et al. Data Overview

- 15 CT scans of “dry” human skulls
  - 9 Male, 6 Female
  - Varying ages (18y-47y)
  - Varying origins (10 European, 2 Australia, 2 Asia, 1 Africa)

Table 1. LIST OF SKULLS

Label	Gender	Age (yr)	Origin	CT System
H1	Female	25	Europe	Siemens Somatom Plus 40
H2	Male	25	Europe	Siemens Somatom Plus 40
H3	Male	20	Europe	Siemens Somatom Plus 40
H4	Female	20	Australia	Siemens Somatom Plus 40
H5	Male	45	Australia	Siemens Somatom Plus 40
H6	Female	20	Africa	Siemens Somatom Plus 40
H7	Male	35	Asia	Siemens Somatom Plus 40
H8	Male	35	Asia	Siemens Somatom Plus 40
H9	Female	23	Europe	Siemens Somatom Plus 40
H10	Male	47	Europe	GE Light Speed 16
H11	Male	23	Europe	GE Light Speed 16
H12	Female	30	Europe	GE Light Speed 16
H13	Female	43	Europe	GE Light Speed 16
H14	Male	31	Europe	Brilliance CT 64-Slice by Philips
H15	Male	18	Europe	Brilliance CT 40-Slice by Philips

Benazzi and Senck. 3D Virtual Methods for Craniomaxillofacial Reconstruction. J Oral Maxillofac Surg 2011.

Benazzi, et al. Virtual Osteotomies

- Virtual osteotomies of the left zygomatic bone performed on each skull
  - 3 cutting planes through:
    - Zygomomaxillary suture
    - Frontosygomatic suture
    - Temporal-zygomatic suture

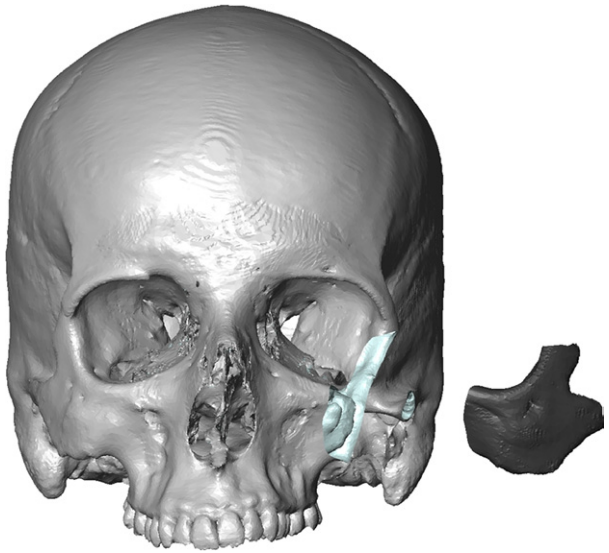

FIGURE 2. Skull H15. Virtual osteotomy of left zygomatic bone.

Benazzi and Senck. 3D Virtual Methods for Craniomaxillofacial Reconstruction. J Oral Maxillofac Surg 2011.

Benazzi, et al. Reconstruction Methods

- Evaluated three approaches
  - Mirroring of the unaffected hemiface
  - Mirroring & Rigid Registration
  - Mirroring & Thin Plate Spline (TPS) warping
- Measure the surface deviation of reconstruction from ground truth

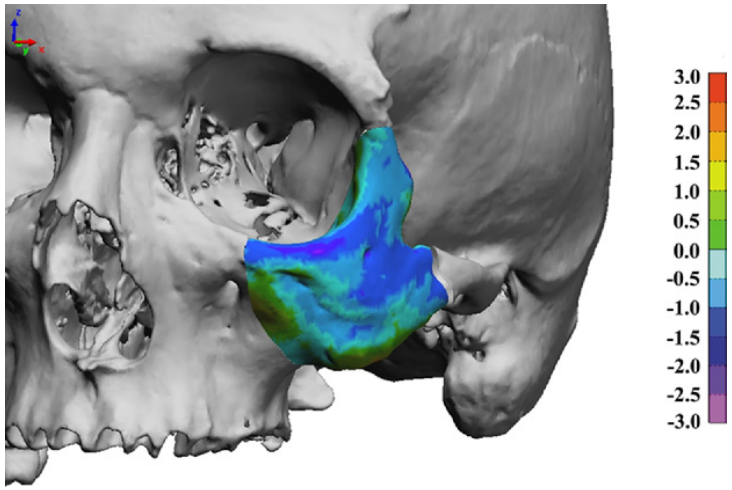

FIGURE 5. Skull H14, anterolateral view. Reconstruction using method 1. Color map illustrating distance between reconstruction and original model (in millimeters).

Benazzi and Senck. 3D Virtual Methods for Craniomaxillofacial Reconstruction. J Oral Maxillofac Surg 2011.

Benazzi, et al. Mirrored Reconstruction

- Use 8 anatomic landmarks to estimate a best-fit mid-sagittal plane
- Reflect the appropriate region about the plane to fill in the missing region

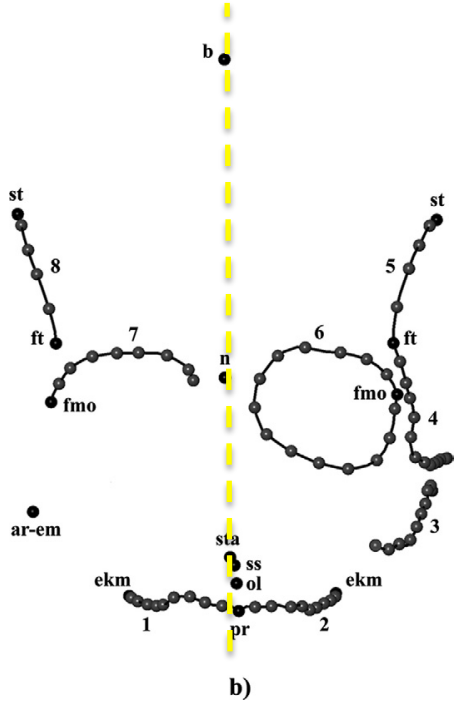

FIGURE 4. Skull H15. Landmarks and curves' semi-landmarks of template; landmarks and curve names listed in Table 2.

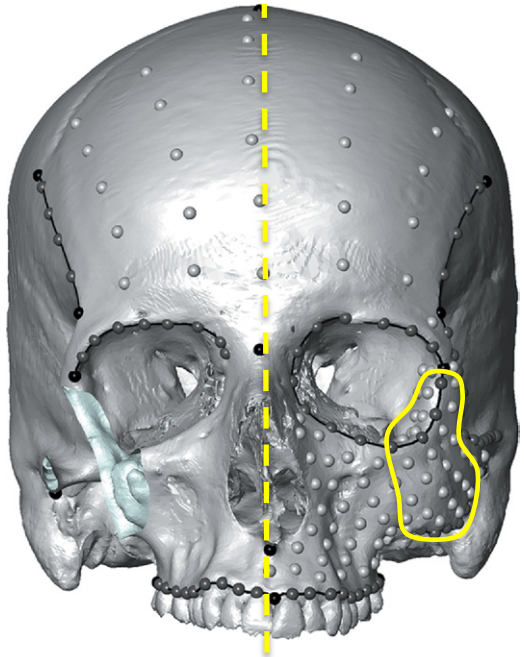

FIGURE 3. Skull H15. *A*, Set of landmarks and curves' semi-landmarks defined on reference model (template). *B*, landmarks and curves of semi-landmarks of template; landmarks and curve names are listed in Table 2.

Benazzi and Senck. 3D Virtual Methods for Craniomaxillofacial Reconstruction. J Oral Maxillofac Surg 2011.

Benazzi, et al. Mirrored Reconstruction Results

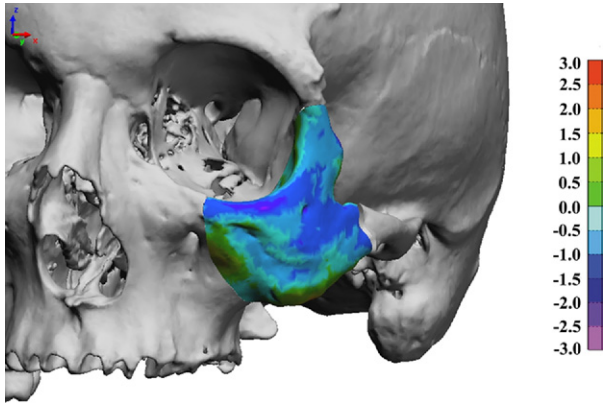

FIGURE 5. Skull H14, anterolateral view. Reconstruction using method 1. Color map illustrating distance between reconstruction and original model (in millimeters).

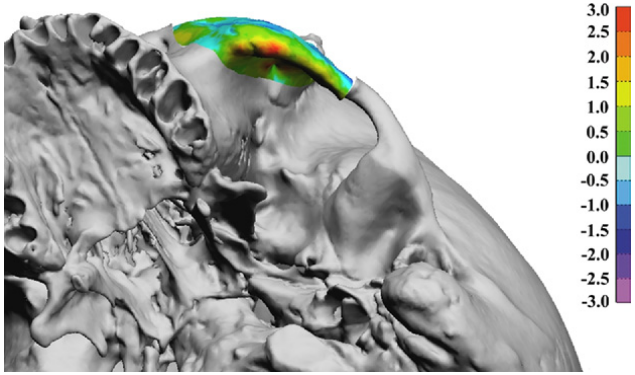

FIGURE 6. Skull H14, basal view. Reconstruction using method 1.

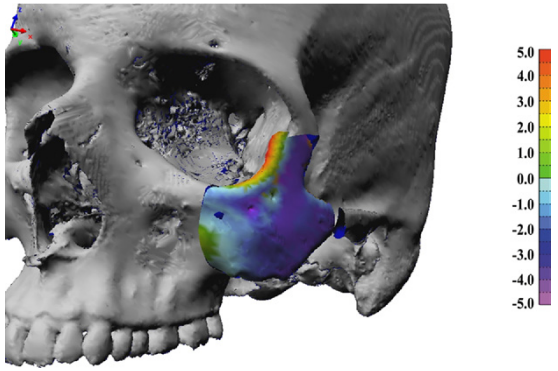

FIGURE 11. Skull H15, anterolateral view. Reconstruction using method 1. Color map illustrating distance between reconstruction and original model (in millimeters).

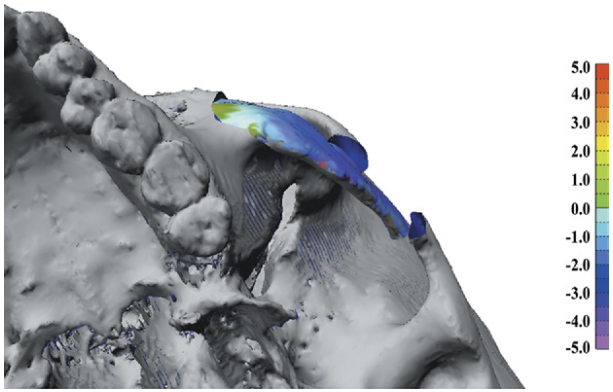

FIGURE 12. Skull H15, basal view. Reconstruction using method 1.

Benazzi, et al. Mirrored & Rigid Registration Reconstruction

- Perform ICP between the destination surface and the mirrored surface

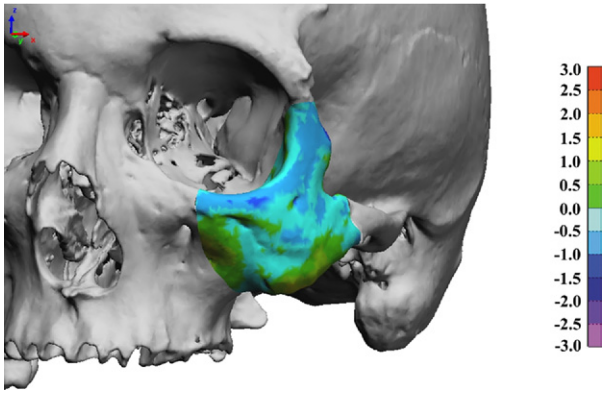

FIGURE 7. Skull H14, anterolateral view. Reconstruction using method 2.

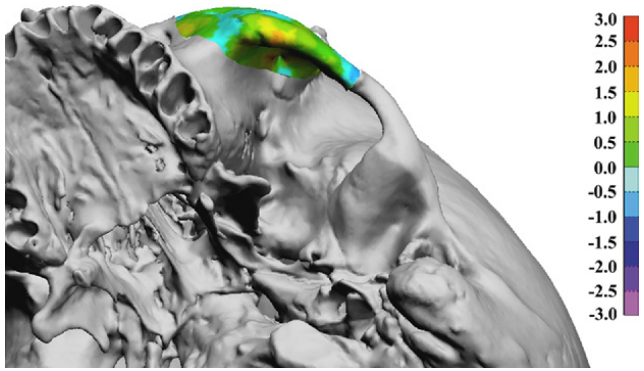

FIGURE 8. Skull H14, basal view. Reconstruction using method 2.

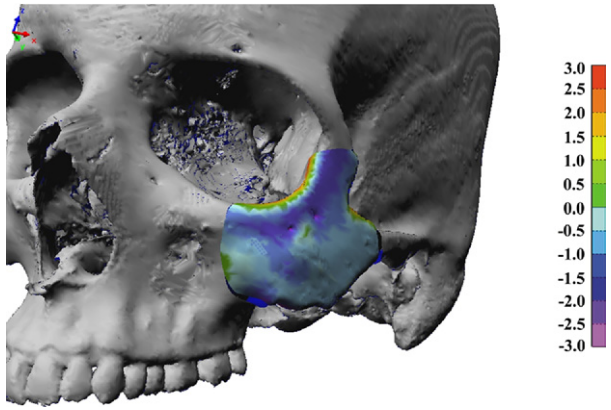

FIGURE 13. Skull H15, anterolateral view. Reconstruction using method 2.

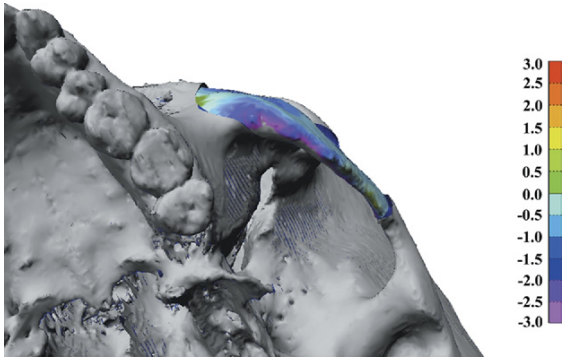

FIGURE 14. Skull H15, basal view. Reconstruction using method 2.

Benazzi and Senck. 3D Virtual Methods for Craniomaxillofacial Reconstruction. J Oral Maxillofac Surg 2011.

Benazzi, et al. Mirrored and TPS Warp Reconstruction

- Identify anatomical landmarks, semi-landmarks, and curves on the mirror surface and incomplete surface
- Project the template landmarks, semi-landmarks, and curves from the mirror surface onto the incomplete surface
  - Allowing "relaxation" of the semi-landmarks and curves
- Warp the mirror template to the incomplete surface using TPS interpolation

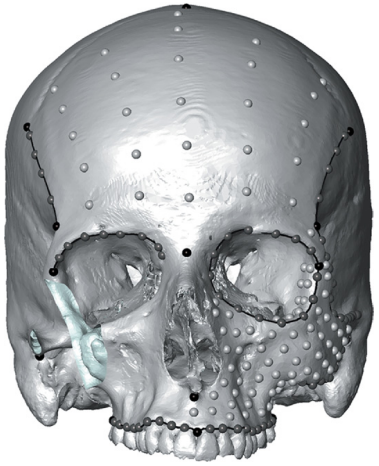

FIGURE 3. Skull H15. *A*, Set of landmarks and curves' semi-landmarks defined on reference model (template). *B*, landmarks and curves of semi-landmarks of template; landmarks and curve names are listed in Table 2.

Benazzi and Senck. 3D Virtual Methods for Craniomaxillofacial Reconstruction. J Oral Maxillofac Surg 2011.

Benazzi, et al. Mirrored and TPS Warp Reconstruction Results

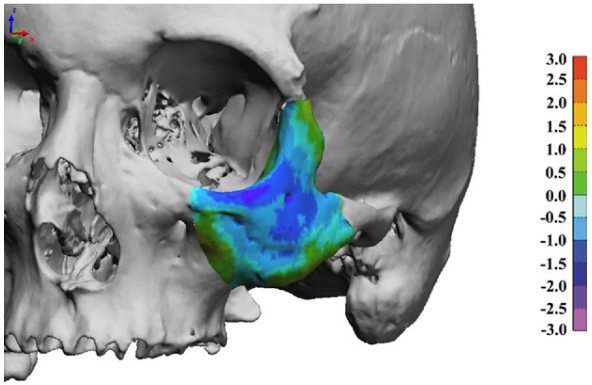

FIGURE 9. Skull H14, anterolateral view. Reconstruction using method 3.

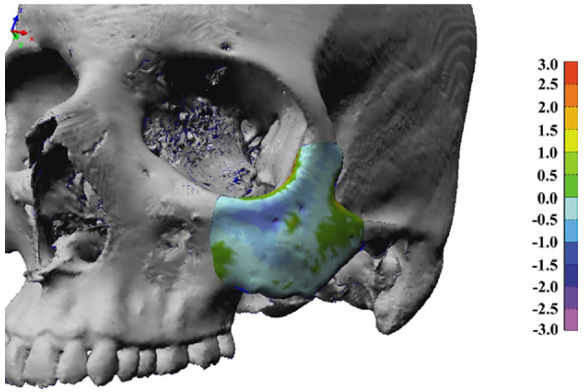

FIGURE 15. Skull H15, anterolateral view. Reconstruction using method 3.

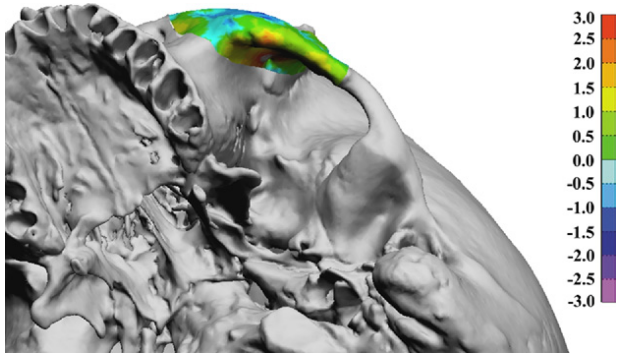

FIGURE 10. Skull H14, basal view. Reconstruction using method 3.

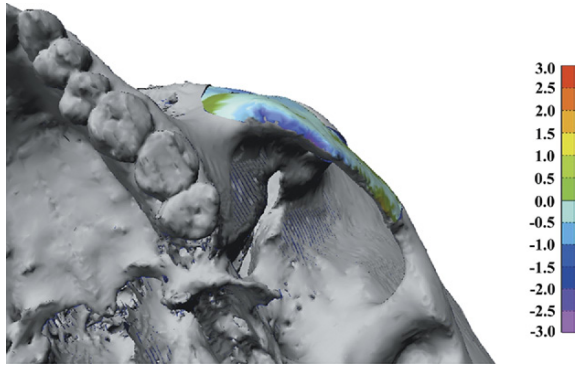

FIGURE 16. Skull H15, basal view. Reconstruction using method 3.

Benazzi and Senck. 3D Virtual Methods for Craniomaxillofacial Reconstruction. J Oral Maxillofac Surg 2011.

Benazzi, et al. Results Comparison Skull H14

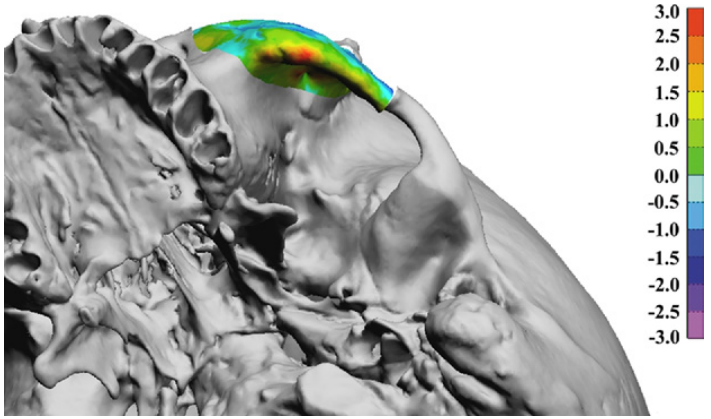

FIGURE 6. Skull H14, basal view. Reconstruction using method 1.

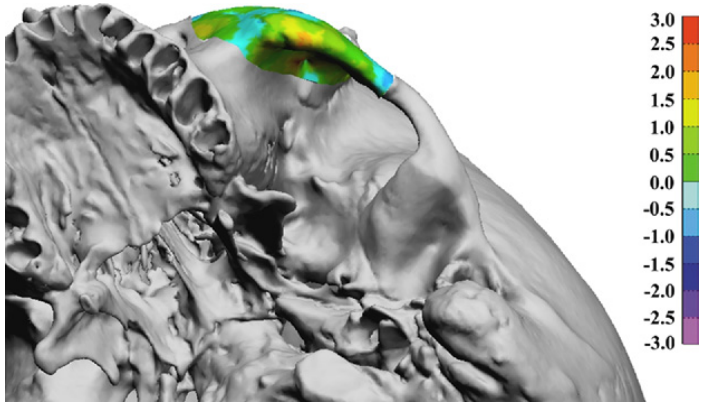

FIGURE 8. Skull H14, basal view. Reconstruction using method 2.

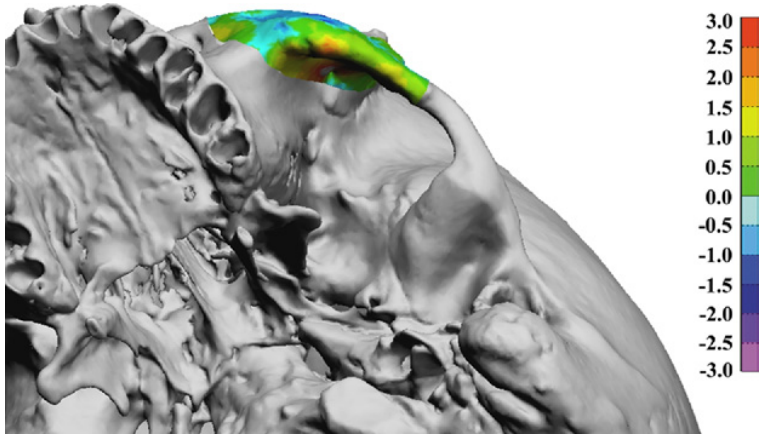

FIGURE 10. Skull H14, basal view. Reconstruction using method 3.

Benazzi and Senck. 3D Virtual Methods for Craniomaxillofacial Reconstruction. J Oral Maxillofac Surg 2011.

Benazzi, et al. Results Comparison Skull H14 (cont.)

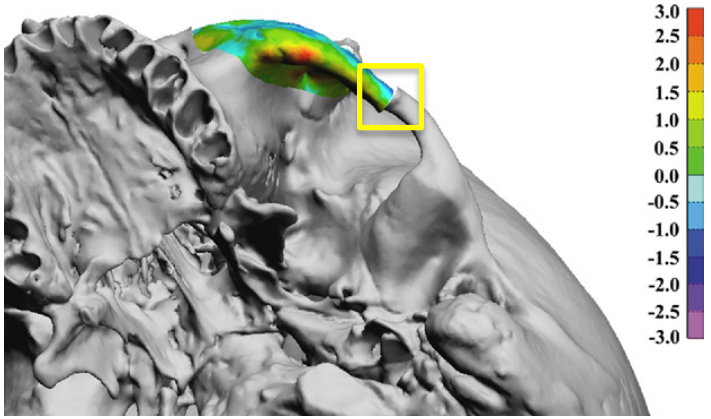

FIGURE 6. Skull H14, basal view. Reconstruction using method 1.

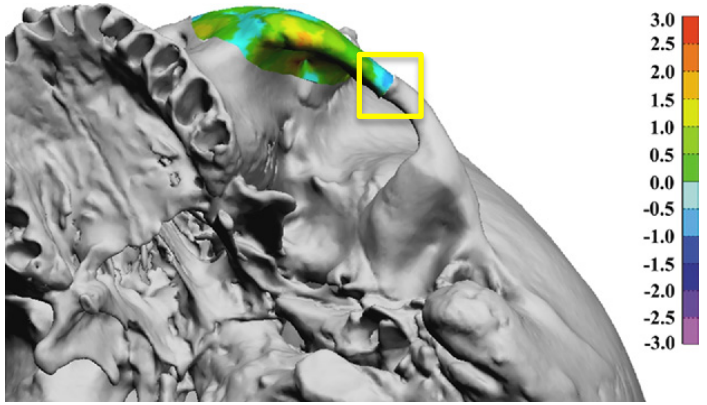

FIGURE 8. Skull H14, basal view. Reconstruction using method 2.

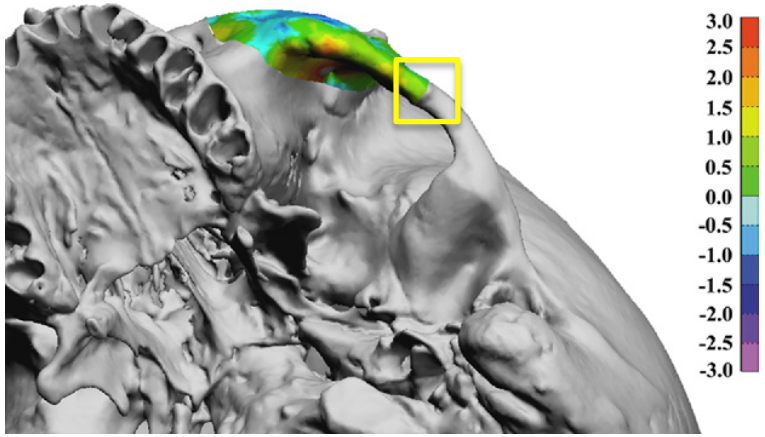

FIGURE 10. Skull H14, basal view. Reconstruction using method 3.

Benazzi and Senck. 3D Virtual Methods for Craniomaxillofacial Reconstruction. J Oral Maxillofac Surg 2011.

Benazzi, et al. Results Comparison Skull H14 (cont.)

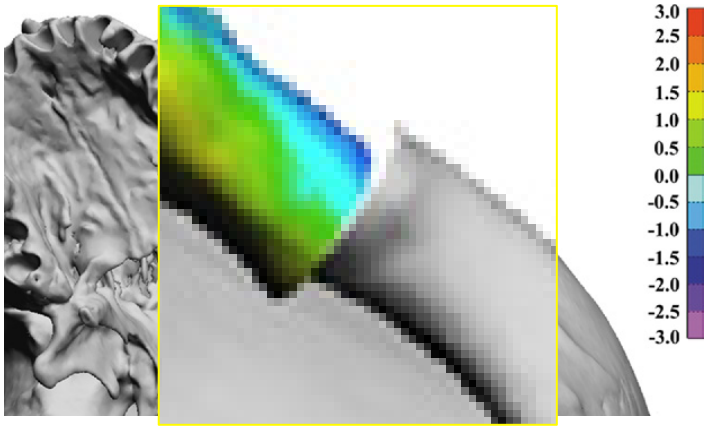

FIGURE 6. Skull H14, basal view. Reconstruction using method 1.

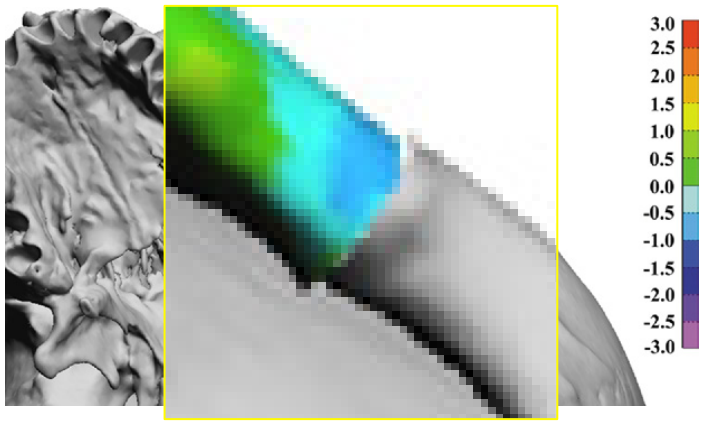

FIGURE 8. Skull H14, basal view. Reconstruction using method 2.

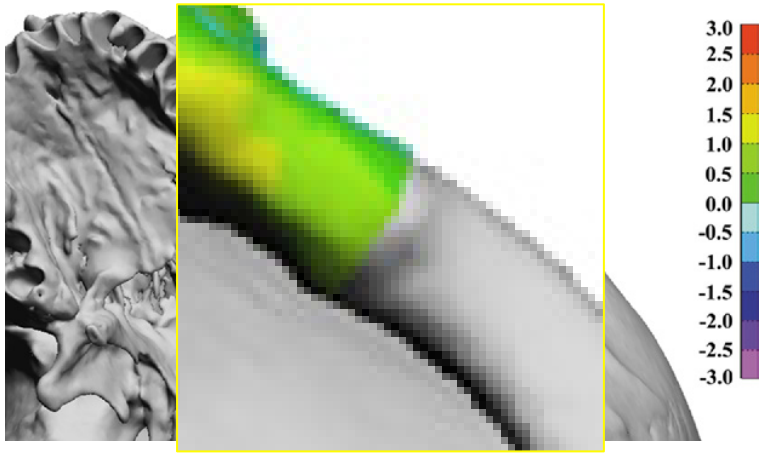

FIGURE 10. Skull H14, basal view. Reconstruction using method 3.

Benazzi and Senck. 3D Virtual Methods for Craniomaxillofacial Reconstruction. J Oral Maxillofac Surg 2011.

Benazzi, et al. Results Comparison Skull H15

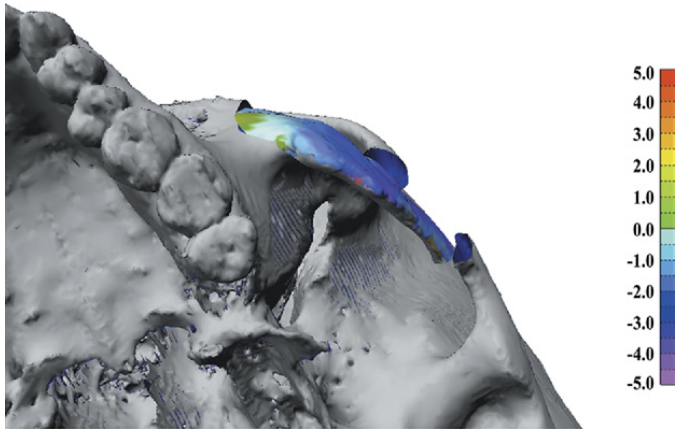

FIGURE 12. Skull H15, basal view. Reconstruction using method 1.

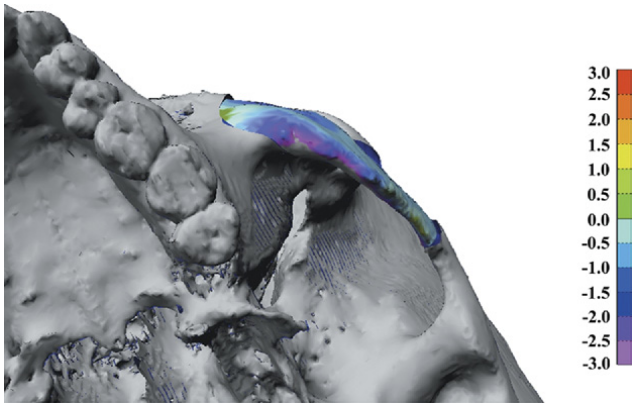

FIGURE 14. Skull H15, basal view. Reconstruction using method 2.

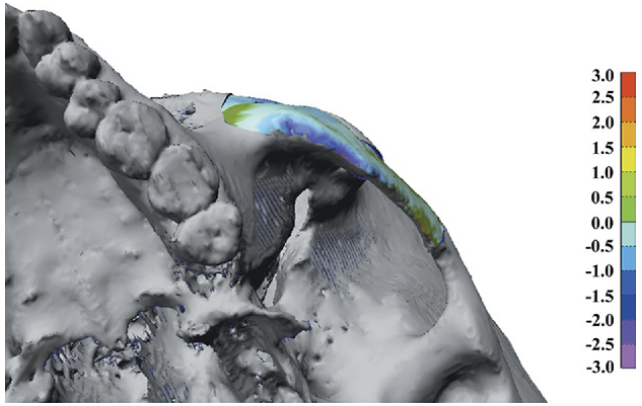

FIGURE 16. Skull H15, basal view. Reconstruction using method 3.

Benazzi and Senck. 3D Virtual Methods for Craniomaxillofacial Reconstruction. J Oral Maxillofac Surg 2011.

Benazzi, et al. Results Comparison Skull H15 (cont.)

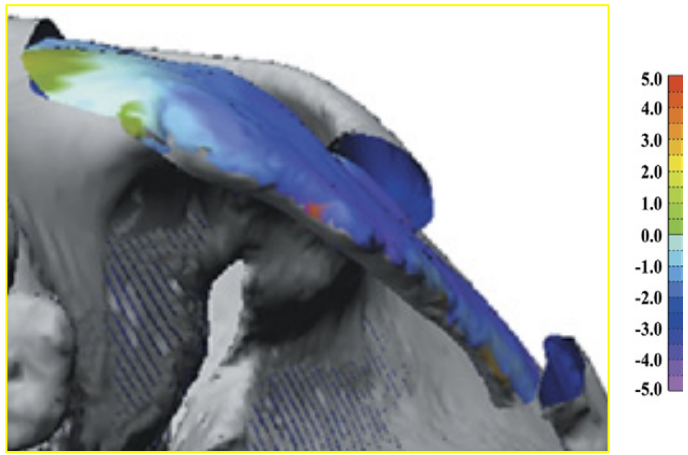

FIGURE 12. Skull H15, basal view. Reconstruction using method 1.

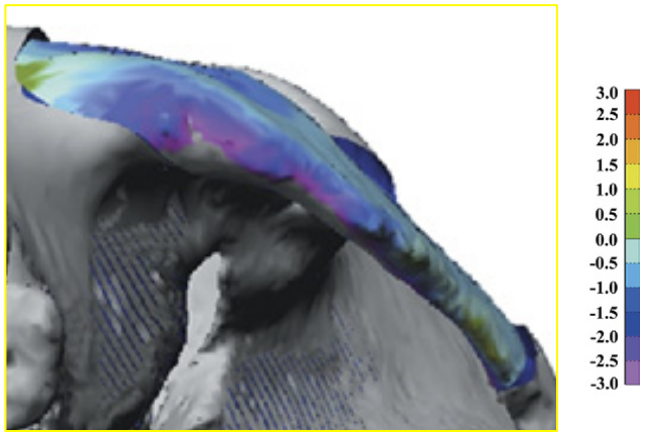

FIGURE 14. Skull H15, basal view. Reconstruction using method 2.

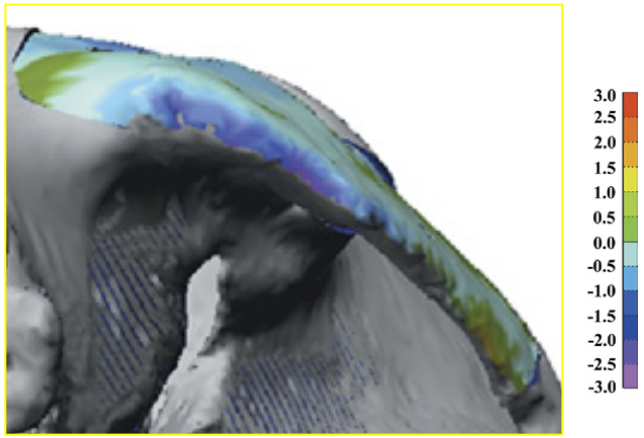

FIGURE 16. Skull H15, basal view. Reconstruction using method 3.

Benazzi and Senck. 3D Virtual Methods for Craniomaxillofacial Reconstruction. J Oral Maxillofac Surg 2011.

Benazzi, et al. Results Summary

- Rigid registration and TPS methods out performed mirroring significantly
- TPS had the smallest standard deviation of surface deviations from ground truth
- Rigid registration and TPS not statistically different
  - Mann-Whitney *U* test

Table 4. INDIVIDUAL ASYMMETRY,* MEAN,† AND STANDARD DEVIATION OF RECONSTRUCTIONS COMPARED WITH ORIGINAL LEFT ZYGOMATIC BONE‡

		Mirror		Mirror Registered		TPS Warping	
List of Skulls	Total Asymmetry	Mean	SD	Mean	SD	Mean	SD
H1	0.00432	−0.497	0.903	−0.032	0.482	−0.142	0.453
H2	0.00837	−0.557	1.411	0.101	0.902	−0.385	0.429
H3	0.00482	0.317	1.105	0.166	0.535	−0.679	0.514
H4	0.00619	−0.249	1.204	−0.047	0.502	0.387	0.402
H5	0.00703	−0.847	1.282	−0.186	0.970	0.342	0.766
H6	0.00477	−0.453	1.425	−0.467	1.254	−0.108	0.714
H7	0.00464	−0.033	0.815	0.142	0.767	0.481	0.499
H8	0.00526	0.078	1.125	0.605	0.836	0.072	0.622
H9	0.00554	0.352	1.551	0.071	0.628	−0.254	0.781
H10	0.00613	1.308	0.478	0.179	0.465	−0.011	0.429
H11	0.00747	−0.861	0.918	−0.113	0.395	0.133	0.352
H12	0.00467	1.602	0.669	−0.268	0.633	0.034	0.387
H13	0.00515	−0.772	0.718	−0.089	0.361	−0.041	0.307
H14	0.00433	−0.352	0.843	−0.044	0.579	−0.280	0.746
H15	0.00746	−1.458	2.085	−0.715	0.993	−0.295	0.627

Benazzi and Senck. 3D Virtual Methods for Craniomaxillofacial Reconstruction. J Oral Maxillofac Surg 2011.

Benazzi, et al. Application to our Project

- The rigid registration method proposed is analogous to using the atlas based extrapolation proposed by Chintalapani
- After performing atlas-to-patient registration, we can use the TPS warping procedure to “smoothly” incorporate the missing anatomy from the atlas
- Will require the manual identification of anatomical landmarks, semi-landmarks, and curves on the patient and registered atlas instance
- Edgewarp 3D: Free software provided by Bookstein, et al. implements this

Kazhdan, et al. Introduction

- Poisson Surface Reconstruction
- Surface reconstruction from oriented points
  - Noisy sensor data from multiple scans
  - Global solution
- Implicit function approach

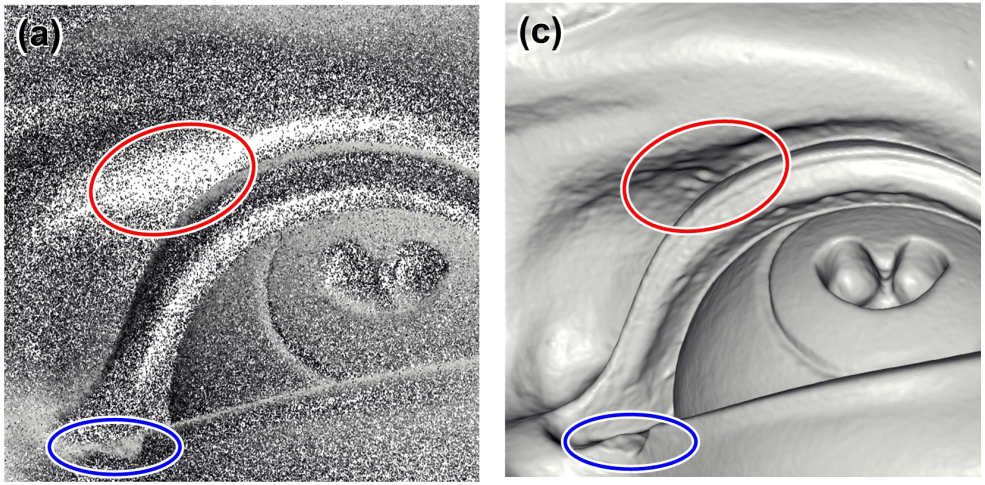

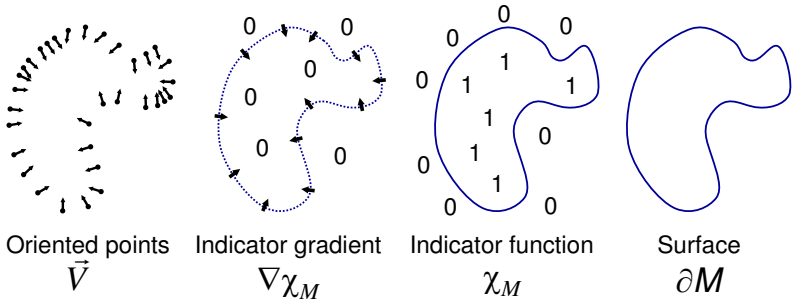

Figure 1: *Intuitive illustration of Poisson reconstruction in 2D.*

Source: Kazhdan, et al. Poisson Surface Reconstruction

Kazhdan, et al. Some Math

- General idea is to super-sample the oriented points into a vector field

$$\sum_{s \in S} |\mathscr{P}_s| \, \tilde{F}_{s.p}(q) \, s.\vec{N} \equiv \vec{V}(q).$$

Sample Points
Size of Surface Partition
Smoothing Filter
Sample Point Normal
Vector Field Coordinate

- Find the best fit indicator function, such that its gradient is equal to the vector field

$$\nabla \tilde{\chi} = \vec{V} \quad \xrightarrow{\text{Divergence Operator}} \quad \Delta \tilde{\chi} = \nabla \cdot \vec{V}$$

Poisson Equation

Source: Kazhdan, et al. Poisson Surface Reconstruction

Kazhdan, et al. Some Math/Implementation Details

- Create an Octree of depth *D*
  - Every sample point falls into a leaf node
- Each node has a "node function"

$$F_o(q) \equiv F\left(\frac{q - o.c}{o.w}\right)\frac{1}{o.w^3}.$$

Octree Node Center

Current Octree Node

Vector Field Coordinate

Base Function

Octree Node Width

- Base function is a compactly supported approximation of a Gaussian

$$F(x,y,z) \equiv (B(x)B(y)B(z))^{*n} \quad \text{with} \quad B(t) = \begin{cases} 1 & |t| < 0.5 \\ 0 & \text{otherwise} \end{cases}$$

- Compute the vector field

$$\vec{V}(q) \equiv \sum_{s \in S} \sum_{o \in \mathrm{Ngbr}_D(s)} \alpha_{o,s} F_o(q) s.\vec{N}$$

Trilinear Interpolation Weights

8 Depth *D* Nodes closest to *s*

Kazhdan, et al. Some Math/Implementation Details

- For each octree node, define an element of the vector *v* as:

$$v_o = \langle \nabla \cdot \vec{V}, F_o \rangle$$

- For each pair of octree nodes, define an element of the matrix *L* as:

$$L_{o,o'} \equiv \left\langle \frac{\partial^2 F_o}{\partial x^2}, F_{o'} \right\rangle + \left\langle \frac{\partial^2 F_o}{\partial y^2}, F_{o'} \right\rangle + \left\langle \frac{\partial^2 F_o}{\partial z^2}, F_{o'} \right\rangle$$

  - *L* is sparse and symmetric

- Solve the following least-squares problem:

$$\min_{x \in \mathbb{R}^{|\mathcal{O}|}} \|Lx - v\|^2$$

- Compute the indicator function as:

$$\tilde{\chi} = \sum_o x_o F_o$$

Kazhdan, et al. Results, Dragon

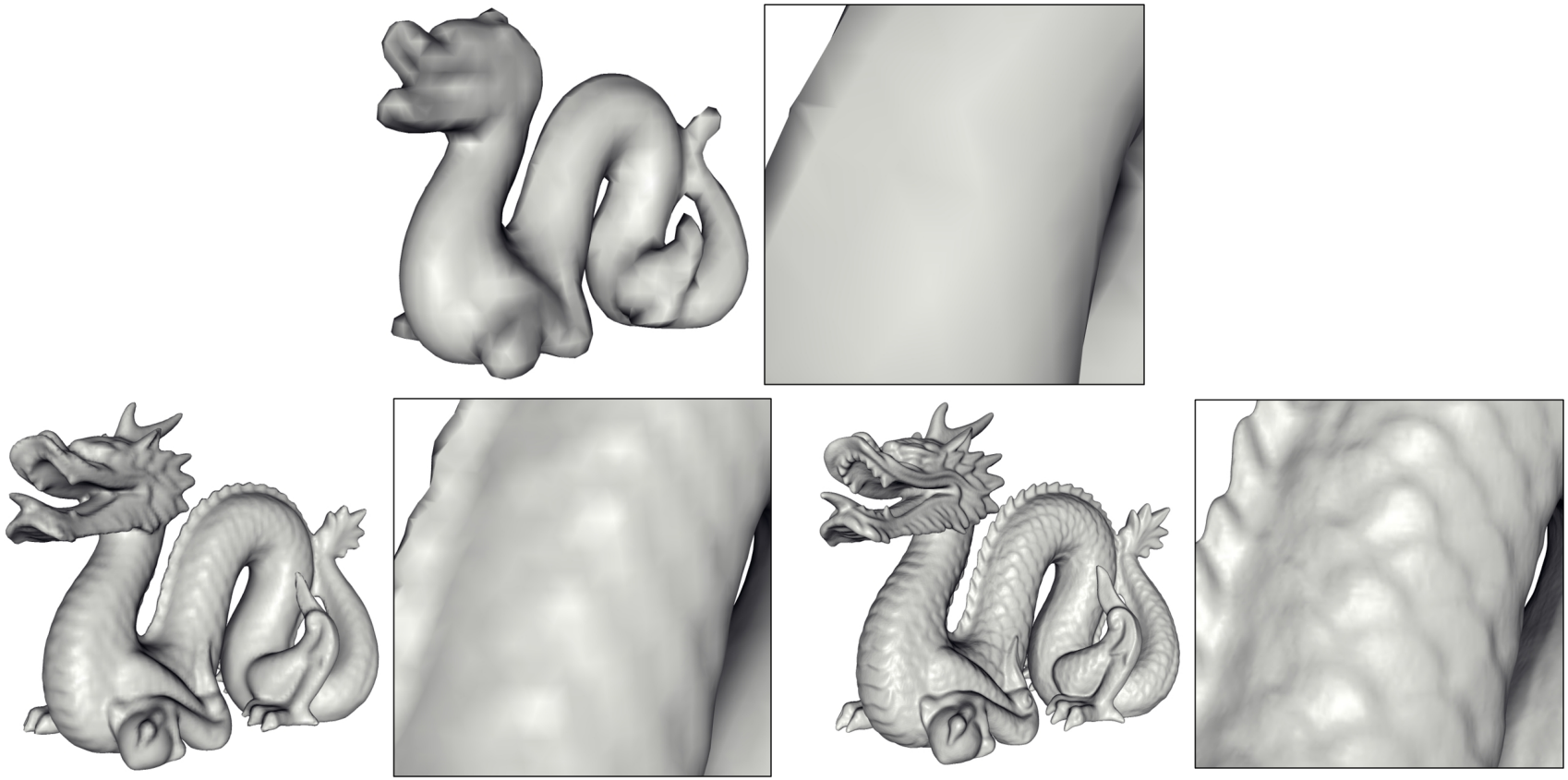

Figure 3: *Reconstructions of the dragon model at octree depths 6 (top), 8 (middle), and 10 (bottom).*

Source: Kazhdan, et al. Poisson Surface Reconstruction

Kazhdan, et al. Results, “Happy Bhudda”

Source: Kazhdan, et al. Poisson Surface Reconstruction

Kazhdan, et al. Results, “Happy Bhudda”

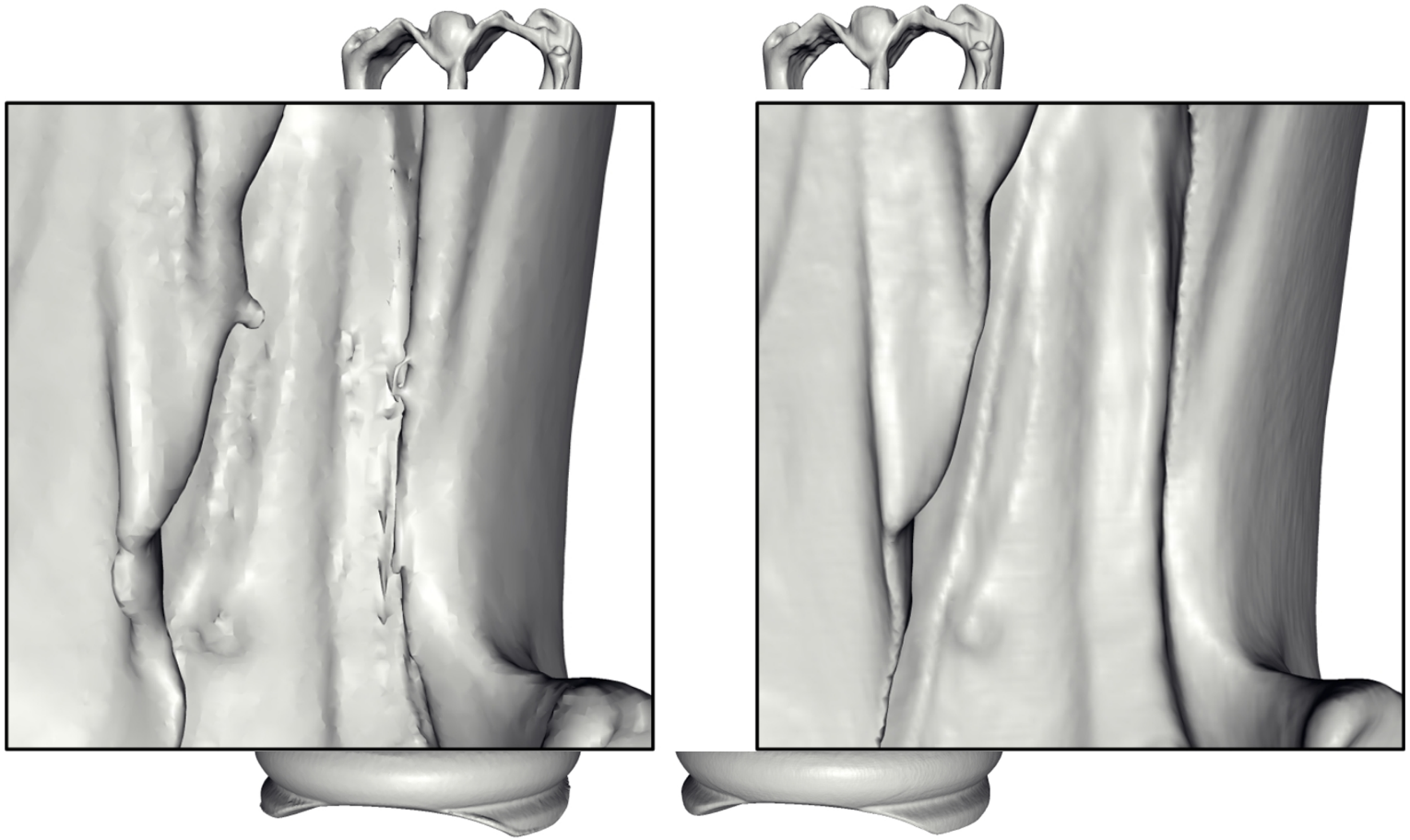

Source: Kazhdan, et al. Poisson Surface Reconstruction

Kazhdan, et al. Results, Michelangelo's David

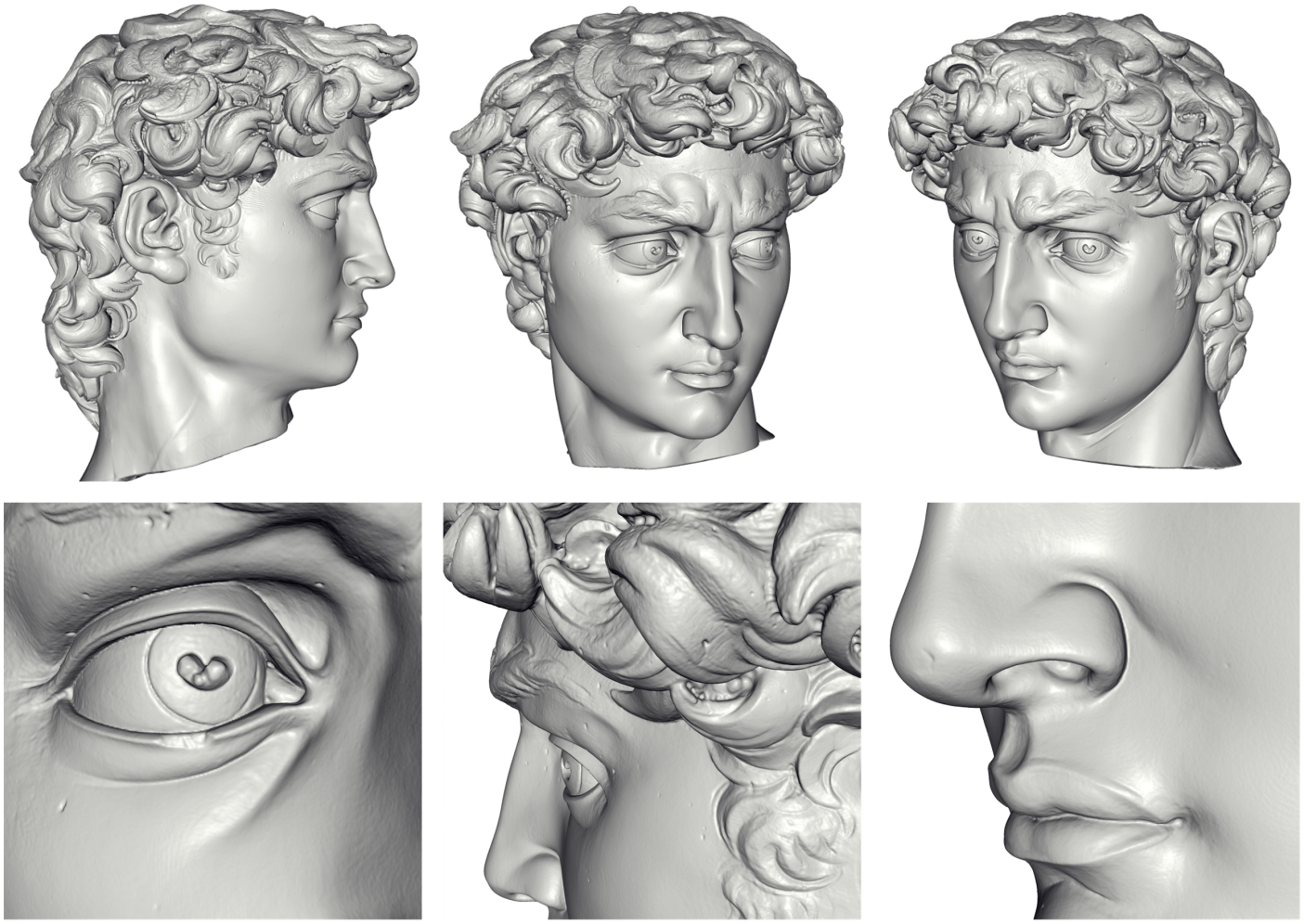

Source: Kazhdan, et al. Poisson Surface Reconstruction

Kazhdan, et al. Application to Our Project

- Perform atlas-to-patient registration
- For each vertex, in the "known" patient and "estimated" atlas instance, compute the inward surface normal
  - Treat these as oriented points

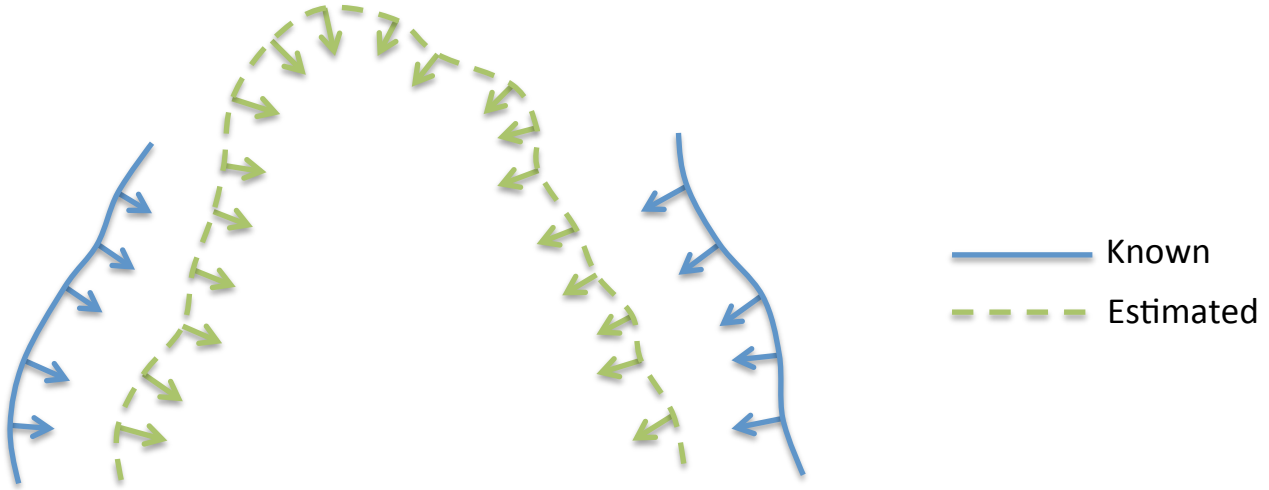

Kazhdan, et al. Application to Our Project (cont.)

- Mask out the estimated points that fall within the “known” region

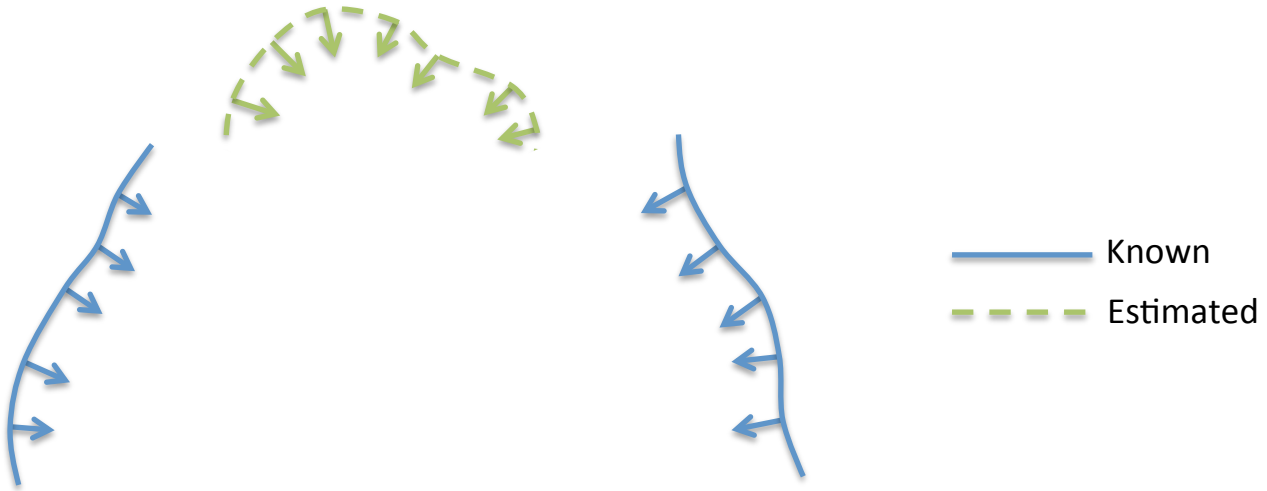

Kazhdan, et al. Application to Our Project (cont.)

- Run Poisson Surface Reconstruction
  - software available on M. Kazhdan's web site

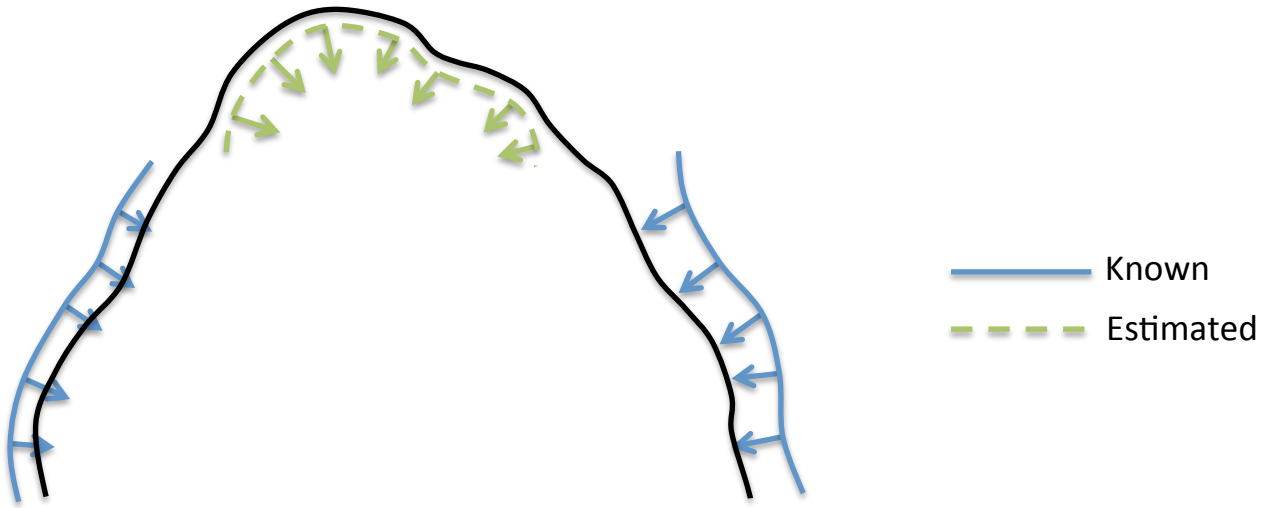

Questions?

“Sliding” Semi-landmarks

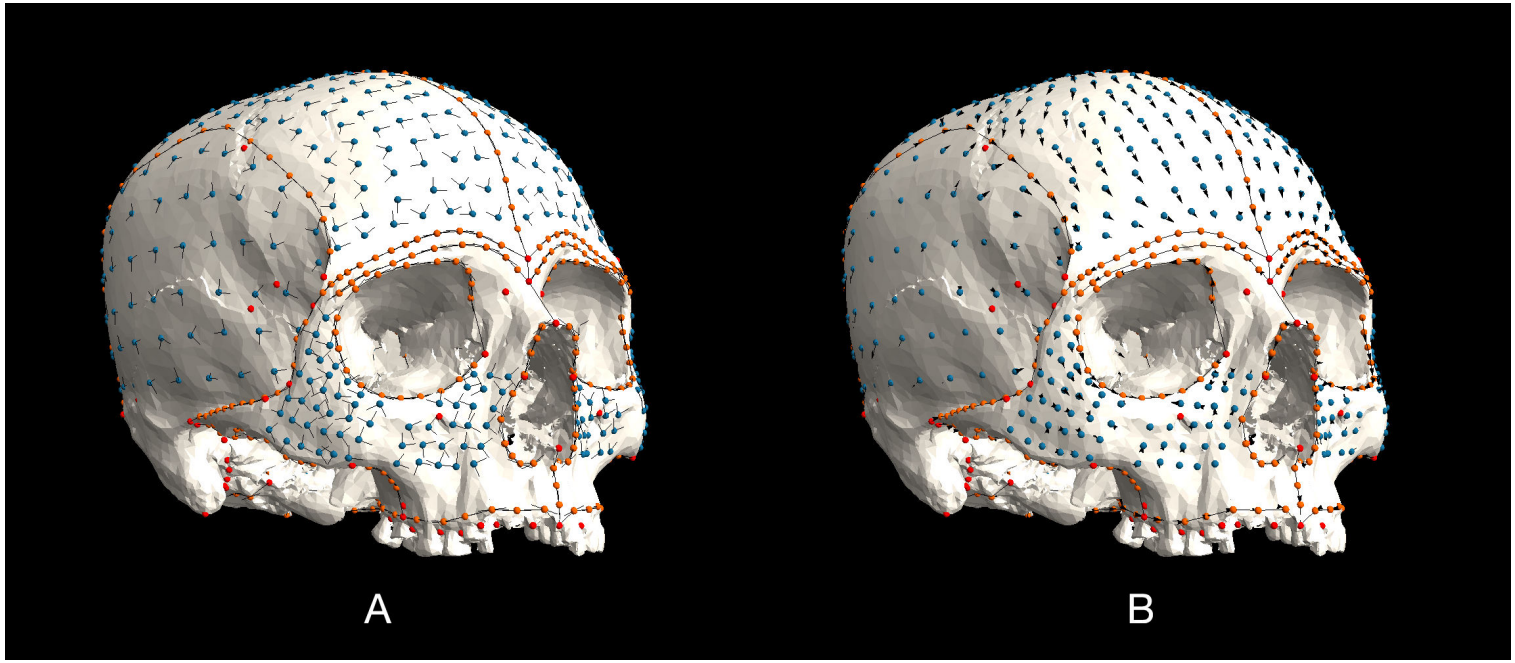

Figure 4 – Landmarks (red), curve semilandmarks (orange), and surface semilandmarks (blue) on a modern human cranium. A: Semilandmarks are allowed to slide along tangents (curves), and tangent planes (surfaces) so as to minimize the thin-plate spline bending energy between this specimen and the Procrustes average shape of the sample. B: After sliding, the semilandmarks are projected back onto the surface. Arrows connect semilandmarks before and after sliding. In this example, the positions of the semilandmarks change only subtly.

Source: Gunz, et al. Semilandmarks: a method for quantifying curves and surfaces